SOURCES OF SHOCK UNSTEADINESS IN SEPARATED SHOCK/BOUNDARY-LAYER INTERACTIONS

L. Agostini,[1] L. Larchevêque,[1] J.-F. Debiève,[1] and P. Dupont[1]
Aix-Marseille Université, CNRS, IUSTI UMR 7343, 13013, Marseille, France

(Dated: 25 August 2014)

Whatever the geometry under consideration, separated flow induced by the interaction between large adverse pressure gradient and boundary layer are often highly unsteady. A LES-based study is presented, which focuses on different unsteadiness-source features in a Mach 2.3 shock reflection with separation. The unsteadiness sources are localised and the path used by the disturbances to spread out from these ones to the whole field are defined. It is shown that phenomena arising inside the recirculation bubble govern the whole interaction, both at low and intermediate frequencies. Indeed the shock motion appears to be the mirror of phenomena found in the separated zone. Moreover, the separated-flow unsteadiness features bear some resemblance to the ones occurring in incompressible flows. An equivalent inviscid scheme of the unsteady interaction is established to describe the whole shock-system unsteadiness at low and intermediate frequencies, as well as the downstream unsteady-pressure field.

Keywords: separated flow, shockwave/boundary-layer interaction, Large-Eddy Simulation

I. INTRODUCTION

Shock wave/boundary layer interactions (SWBLI) are ubiquitous in aeronautical applications. Whatever the flow configuration under consideration (compressions ramps, shock reflections, blunt-fin or over-expanded nozzles), separation-shock displacement arise at low frequency. Fully separated interactions have been widely studied in the past by means of experiments[1–6]. More recently, additional information has been obtained from Direct Numerical Simulations[7] (DNS) or Large-Eddy Simulations[8,9] (LES). Nevertheless the origin of the low-frequency shock displacements is not yet clearly established.

In high Reynolds cases, upstream perturbations have been shown to influence separation-shock motions[6,10,11]. However these experiments considered nearly attached/incipient-separation configurations for which no reverse flow could be observed from Particle Image Velocimetry (PIV) measurements in a time-average sense.

Comparisons between two incipient-separation cases, respectively at low and high Reynolds number[12,13] confirm a that the separation-shock displacement is correlated with the upstream-boundary-layer unsteadiness but also with unsteadinesses located in the interaction region developing downstream the separation shock. In the separated cases, for which a well defined mean-recirculation region is observed, recent results obtained for low Reynolds number SWBLI[5,7,14] have shown that the low-frequency shock unsteadiness has to be related to the downstream part of the separated flows.

Several models derived from experimental data as well as from numerical simulations were introduced in order to define the low-frequency unsteadiness sources, see Morgan *et al.*[9] for a recent review. Touber and Sandham[15] and Priebe and Martin[16] suggest they have to be related to an instability of the separation bubble, induced by a stationary global mode, leading to self-sustained oscillations of the interaction region and to specific time evolution of the skin friction coefficient. Nevertheless, different results are proposed by Touber and Sandham[17]: using several hypotheses based on data from a LES of a 8° shock reflection, theses authors derived an equivalent low-pass filter system, as previously suggested by Plotkin[18] and Poggie and Smits[19].

On the opposite, Piponniau *et al.*[20] suggest to relate the observed low-frequency un-

steadiness of the separated bubble to the mass entrainment across the mixing layer which develops between the separated region and the outer supersonic flow. This model suggests a direct link between the Kelvin-Helmholtz-like convective structures of the mixing layer and the low-frequency unsteadiness of the separated region. The convective structures are associated with what will be hereafter referred to as medium frequencies since they are one order of magnitude higher that the low frequencies related to the bubble breathing as well as they are one order of magnitude lower than the energetic eddies of the upstream boundary layer. The development of these structures were identified from unsteady wall-pressure measurements[5] and from PIV data[14]. The low-frequency breathing of the separation bubble and shock displacement were found to be linked to each other, and some evidences of similarities between the separated regions in SWBLI and incompressible separated flows were given, although significant influence of the compressibility effects are expected in the mixing layer. The model was able to give some relevant scaling for the low-frequency shock unsteadiness in various SWBLI configurations, however detailed description of the process was not addressed.

Moreover, several experimental results obtained in various SWBLI are not yet clearly explained by these different models. For example, it is known for decades that specific phase relationships are observed from unsteady wall-pressure measurements[1,2,5]. It was shown that, whatever the geometry (compression corner or shock reflection) and Mach number ($1.5 < M < 5$) are, strong correlation at low frequency occurs between the wall pressure fluctuations created by the shock unsteadiness and the wall pressure fluctuations downstream of the shock. The initial region of the interaction exhibits in-phase pressure fluctuations while the region near the reattachment point presents anti-phase pressure signals. These two regions are separated by a zone of null correlation whose origin is not yet well established.

The aim of this paper is to use recent LES of the shock reflection based on experiments from the IUSTI laboratory, obtained over a long time with respect to the low-frequency unsteadiness (typically more than 150 cycles have been sampled) so as to generalise experimental observation at the wall to the whole flow field in order to:

- localize the source of the interaction unsteadiness at low and medium frequencies,
- describe the spatial links leading to the observed pressure fluctuation levels in the field,
- give a simple equivalent scheme, involving the subsonic near-wall region as well as the supersonic external flow with the shock system and the downstream region.

The paper is organized as follows. In section II, the numerical method and aerodynamic parameters are reminded, and validation versus experiments are presented. In section III, the spatial links between the separated bubble and the external flow are identified. In Section IV, the near-wall pressure unsteadiness will be investigated and compared to incompressible separated flows. This analysis will be extended to the supersonic region of the interaction in section V. An equivalent simple inviscid model, summarising the whole observations and results, is introduced in section VI. Lastly, properties shared by both incompressible and compressible separations will be discussed and the inviscid aforementioned model will be extended to the medium-frequency unsteadiness in section VII

II. FLOW PARAMETERS AND COMPUTATIONAL DETAILS

A Mach=2.3 shock reflection on a flat plate is considered. Experiments are set up in IUSTI's supersonic-wind tunnel and LES of the flow is achieved at the same Reynolds number as the experiments, namely $Re_{\delta_2} = 5000$, where δ_2 stands for the momentum thickness of the upstream boundary layer. The experimental set-up and main results have been widely described in previous works[5,14,20–23]. The upstream aerodynamic parameters are given in table I. An interaction with a flow deviations of 9.5°,corresponding to an noticeable separation, is considered for the present work. A schlieren picture of the interaction is printed

TABLE I. Main aerodynamic parameters of the interaction

M	Re_{δ_2}	$U_\infty[ms^{-1}]$	$\delta_0[mm]$	δ_2[mm]	$P_0[Pa]$	$T_t[K]$	Flow Deviation[°]
2.3	5.1×10^3	557	11	0.96	0.5×10^5	293	9.5

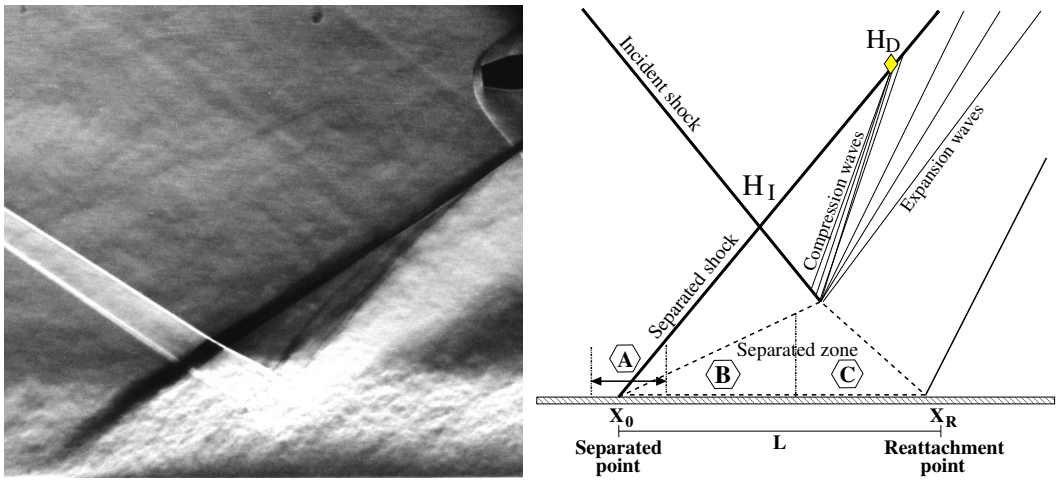

(a) (b)

FIG. 1. (a) Schlieren picture of the shock boundary layer interaction carried out in IUSTI's wind tunnel[20]. (b) Sketch of the shock boundary layer interaction.

in figure 1(a) and its main features are sketched in figure 1(b). The experimental set-up yields some significant three dimensional organisation of the interaction[21], whose origin has been identified from numerical simulations as being the side wall boundary layer[24,25]. Mean turbulent-velocity fields, as well as time properties of the flow have been derived from PIV[14,20], hot wire and unsteady wall-pressure measurements[5,22]. For both the experiments and the LES, low-frequency unsteadiness of the separation shock has been observed and has been associated with a characteristic non-dimensional frequency, or Strouhal number, such as:

$$S_L = \frac{fL}{U_1} \simeq 0.03 \tag{1}$$

where f is the frequency of the pressure fluctuations at the mean location of the separation-shock foot (which is defined as the location where the standard deviation of the wall pressure fluctuations is highest), L is the interaction length and is U_1 is the external velocity downstream the incident shock. The length L is defined as the distance between the mean location of the separation-shock foot, denoted X_0, and the extrapolation down to the wall of the incident shock.

The LES whose results are used in this article were designed in order to achieve long-time integration encompassing a large number of low-frequency cycle. Consequently the three-dimensional organisation of the flow was not taken into account and periodicity conditions were used in the spanwise direction, as in previous LES of similar flows[8,26]. Two computational domains were tested, both having a length equal to $5.6\,L$. The first one had a span equal to $1.6\,\delta_0$, following Garnier et al.[26], whereas the second one was enlarged, with a span equal to $11\,\delta_0$, a value larger than the one used by Touber and Sandham[17]. The same grid resolution, suited for wall-resolved LES, with $\Delta x^+ \simeq 40$, $\Delta z^+ \simeq 16$ and $y_1^+ \simeq 0.9$, was used for both of the domains. An additional computation has been performed for the narrowest domain using a refined grid, with $\Delta x^+ \simeq 30$, $\Delta z^+ \simeq 12$ and $y_1^+ \simeq 0.8$.

For all these computations, the effect of subgrid scales on the resolved ones was taken

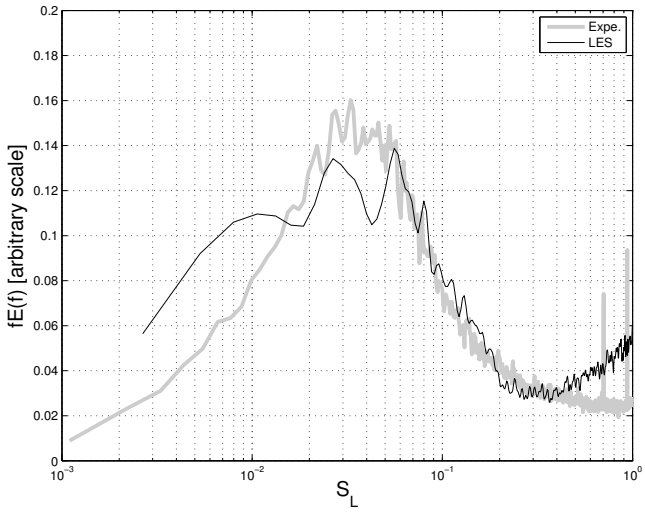

FIG. 2. PSD of the wall-pressure fluctuations in the vicinity of the mean location of the separation-shock from LES (solid black line) and experiments (solid grey line). The Strouhal number S_L is defined by equation 1.

into account using the selective mixed-scale model[27]. Ducros' sensor[28] was used in order to switch from a centered scheme in the turbulente-dominated region to a Roe dissipative scheme in the shock region, so that the numerical dissipation does not mask the effect of the subgrid model. An unsteady condition based on a Synthetic Eddy Method[29] was used at the inflow boundary, located $11\,\delta_0$ upstream of the interaction region, thus resulting in a fully–turbulent boundary layer upstream of the separation. Characteristic–based non–reflecting conditions were used for the upper and outflow boundaries.

Details on validation process including comparisons with experimental data and between the additional simulations with refined and enlarged meshes can be found in Agostini *et al.*[30]. Specifically, it is shown that the spatial as well as the temporal flow organisations are accurately reproduced, despite a slight under-estimation of the interaction length found in the simulations with respect to experimental results. The difference is of about 15%, whatever the flow deviation under consideration and recent works have shown that this difference is likely due to some side effects in the experiments, associated with the finite span of the wind tunnel[24]. Nevertheless, it is shown in that the space and time flow properties, when normalised by the interaction length, are accurately reproduced[30].

Quite long computations over at least 150 low-frequency cycles allowed to derive Power Spectral Densities (PSD) of the pressure fluctuations along the interaction which compared very well with experimental results. The characteristic low-frequency shock motion of Strouhal number close to 0.03 were obtained for all cases of flow deviations that have been tested, including the 9°5 case under consideration in this paper. This property is illustrated in figure 2, where the experimental and numerical PSD of the pressure in the vicinity of the mean position of the foot of the separation shock are presented in case of the 9°5 flow deviation.

Most of the available experimental results concerning the space-time SWBLI properties have been derived either from unsteady wall-pressure measurements or from in-field Hot-Wire measurements[1,2,5]. As recalled in the previous section, several spectral properties (PSD, phase and coherence relationships) where derived, but were mainly limited to wall measurements. Recently, complementary data have been obtained from *Dual-PIV* measurements[12,31,32] and from Linear Stochastic Estimation analysis, applied on simultaneous measurements of unsteady wall-pressure and velocity fields by PIV[33]. These results confirm the low-frequency correlations between the shock motion and the downstream interaction region derived from wall-pressure and hot wire measurements. In the next sections,

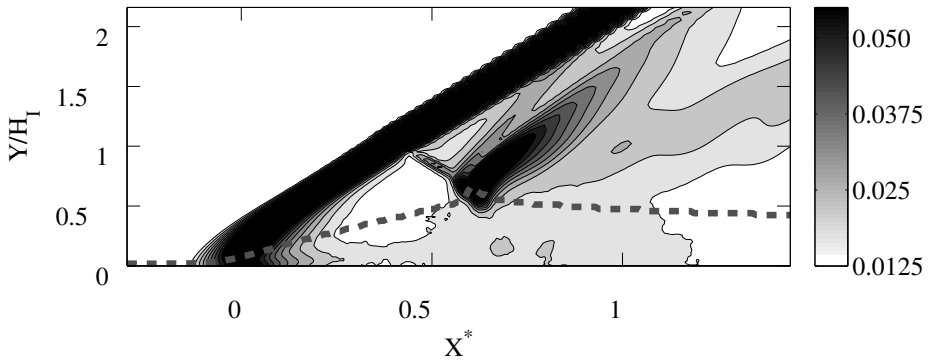

FIG. 3. Root Mean Square values p^*_{LF} of the low-pass filtered ($S_L < 0.08$) pressure fluctuations. Contour levels have been clipped to 10% of the maximum value in order to make the plot legible. The streamwise and wall-normal coordinates have been respectively normalized by L and H_I (see figure 1(b) and equation III for definitions) and the dashed line denotes the sonic line.

space-time resolved computations data are used to generalise these results to the whole field in order to identify the different unsteadiness sources and determine how they influence the various flow regions. Velocity, density and pressure data in wall-normal planes are stored with a 200 kHz sampling rate. This frequency has been controlled to be sufficient to avoid any significant aliasing effect for frequencies lower that 20kHz, which is sufficient to analyse the interaction region.

III. SPATIAL LINKS BETWEEN THE SEPARATED BUBBLE AND THE EXTERNAL FLOW

The low-frequency unsteadiness of the shock displacements generate large pressure variations, related to the pressure jump across the shock, denoted Δp_s: they induce a sharp increase of the pressure fluctuations such as their RMS values are equal to half of Δp_s[5,23,34]. As these fluctuations are not directly produced by turbulent phenomena, they will be referred to as *intermittent*. Similar comments apply for the expansion-wave region, where pressure fluctuations are generated by the oscillations in space of the pressure gradient.

The "intermittent" fluctuations associated with the separation shock and expansion wave are found dominant in figure 3, where a map the RMS values of the low-pass filtered pressure p_{LF}, normalized by the upstream static pressure P_0 as $p^*_{LF} = p_{LF}/P_0$, is plotted. The non-dimensional cutoff frequency of the low-pass filter is $S_{Lc} = 0.08$. This frequency range encompass the low-frequency shock motions whose power spectra are centred around $S_L \simeq 0.03$, see figure 2). The longitudinal dimensionless coordinate X^* is defined by considering the location of the separation-shock foot and the length of the interaction, defined in figure 1(b), as:

$$X^* = \frac{X - X_0}{L}$$

The other regions of the flow display much lower low-frequency pressure fluctuations. In concordance with experimental results[5], no significant pressure fluctuations are identified for the upstream boundary layer in this frequency range. It has to be mentioned that any influence of "super-streaks" on the interaction unsteadiness, as reported in the literature[11,35], cannot be expected in the present simulations. Indeed, a Synthetic Eddy Method is used to generate the turbulent boundary condition at the inflow and the resulting boundary layer develops over a distance of 11δ. This distance is at least three times smaller than the length

of these "super-streaks", equal to about 30δ[36].

Low levels of low-frequency pressure fluctuation are also found unexpectedly in the interaction region, in the zone located immediately downstream of the separation shock and above the separated bubble, with RMS values lower than 1.25×10^{-2} P_0. RMS values increase when moving down into the separation bubble but still remain weak in that region, labelled B in figure 1(b). Downstream of it, up to the reattachment point, in the region of the bubble denoted by C in figure 1(b), the low-frequency fluctuation levels rise smoothly up to a value of about 3.2×10^{-2} P_0 that is approximatively equal to the ones found in the outer flow, downstream of the expansion wave.

The strongest low-frequency pressure fluctuations found in the interaction region, apart from the separation-shock and the expansion-fan zones, are located in a narrow band upstream of the expansion fan and are spreading out from the impingement of incident shock on the shear layer. Henderson[37] has shown that when a shock impinges a boundary layer, their interaction can not be restricted to a simple reflection. The incident shock is refracted through the boundary layer and such a refraction result either in reflected compression waves, in reflected expansion waves, or in both of them, depending on the intensity and the angle of the incident shock and on the features of the upstream boundary layer. The latter process is bound to occur in the interaction studied in this paper since, based on the schlieren picture of figure 1(a), compression waves are found in that narrow region. It will be shown later in part V that these unsteady compression waves play a key role in the pressure equilibrium within the interaction.

The study of the RMS pressure values at low frequencies shows that the interaction can be split in several parts associated with different level of RMS pressure. In order to understand this spatial organization, the coherence field between the pressure fluctuations and the separation-shock displacements have been derived from the time-resolved LES data. The shock motion is estimated, for a given altitude, from the streamwise location of the maxima of the pressure variation induced by the separation shock, detected by computing the pressure derivative in the direction normal to the separation shock[30]. The time evolution of the instantaneous shock location can then be used to put into evidence the relationship between the shock motion and the interaction region. The coherence function, defined by:

$$Coh(f) = \frac{|\widehat{S_{s,p}}|}{\sqrt{\widehat{S_s}\widehat{S_p}}} \tag{2}$$

where $\widehat{S_{s,p}}$ is the cross spectrum between the shock location s and the pressure fluctuations p and $\widehat{S_s}$ and $\widehat{S_p}$ are the PSD of s and p, respectively, highlights the links between the pressure fluctuations and the shock position, independently of any phase between the two signals. Its value range from 0 to 1, corresponding respectively to uncorrelated signal and fully correlated signals at the frequency f.

The coherence function between unsteady wall pressure induced by the separation-shock displacements and the streamwise distribution of wall-pressure fluctuations have been widely documented from experimental works for compression ramps[1,2,38] and for shock reflections[5,14,39]. These works have highlighted that wall-pressure fluctuations in the second part of the separated zone are highly correlated and are in anti-phase with pressure fluctuations occurring at the separation-shock foot. Theses observations have also been confirmed from numerical simulations, DNS[40,41] as well as LES[42].

With respect to these studies, the use in the present work of the shock location rather than the wall pressure allows the extraction of the genuine relationship between the shock unsteadiness and the whole interaction. The coherence-coefficient map associated to the Strouhal number of 0.03 are shown in figure 4 . The white star marks the reference altitude at which the streamwise location of the shock is estimated. The maximal values are in black and the minimal in white. The wall streamwise distribution of the coherence coefficient has the same features than the previous results mentioned above. Nevertheless, from numerical simulations, these phase relationships can be extended from the wall to the whole field, thereby to define and to figure out the zones of influence and the links between each of them.

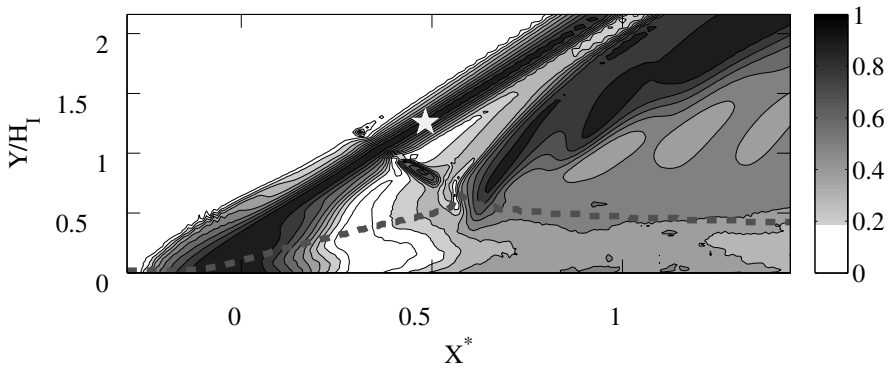

FIG. 4. Map of the coherence between the shock displacement at the altitude denoted by a star and the pressure fluctuation p for the typical normalized frequency $S_L \simeq 0.03$ associated with the low-frequency unsteadiness of the interaction. The dashed line denotes the sonic line.

For the low frequency range under consideration, no correlation between the separation-shock displacements and the upstream pressure fluctuations are observed while the largest coherence-coefficient level is found in the region of the separation-shock displacement. The interaction is split into two parts strongly correlated, separated by an intermediate region corresponding to a gap of coherence.

Similar results have been obtained from the low-pass-filtered cross correlations[30]. These authors showed that pressure fluctuations in the second part of the interaction are in phase with the low-frequency shock displacements, and thus are in anti-phase with the induced pressure variations since, when the shock moves in the upstream direction, *i.e.* for decreasing values of x, the pressure at the shock mean position goes up whereas when the shock moves in the opposite direction (downstream), the pressure level goes down. The results presented in this section confirm that the separation-shock dynamics at low frequencies is governed by phenomena occurring inside the separated zone. Moreover, the fact that the interaction is split into two regions on each side of a coherence gap suggests that two specific dynamics are at work within the bubble. Pressure fluctuations features occurring in the separated zone are described more thoroughly in the next section in order to understand the origin of this coherence gap.

IV. PRESSURE UNSTEADINESS IN THE SUBSONIC DECELERATED REGION

A. Wall Pressure fluctuations

It was mentioned in section III that the large fluctuations encountered in the region spanned by the motion of the separation shock were *intermittent* in nature. It is consequently desirable to try to remove them in further analyses since they are associated with purely kinematic effects and are consequently a bad indicator of the flow dynamics within the interaction. The removal can be achieved by considering data in the frame associated with the separation shock rather than in the laboratory frame.

Using the time evolution of the separation-shock location, the low-frequency wall-pressure RMS values are recast in the moving frame associated with these locations. The resulting streamwise profile is plotted in figure 5 alongside with its counterpart computed in the laboratory frame. The dimensionless pressure $P^* = (P - P_0)/P_0$ is also reported on the figure. As expected, the large peak of RMS pressure values located in the shock-displacement region when considering the laboratory frame vanishes in the frame associated with the separation shock. It clearly confirms the intermittent nature of these pressure fluctuations, related to

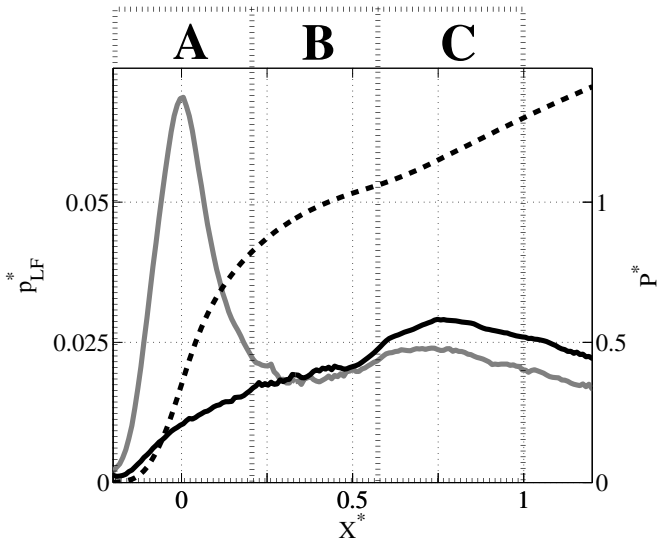

FIG. 5. Streamwise distribution of the RMS values p^*_{LF} of the low-frequency wall-pressure; solid grey line: laboratory frame; solid black line: moving frame associated with the separation-shock frame; dashed line: mean pressure in the laboratory frame. Regions A, B and C are defined in section IV.

the large pressure gradient across the separation shock. Downstream, where the pressure gradient is milder, the values obtained in the separation-shock and wind-tunnel frames are close to each other, both increasing up to $3 \times 10^{-2}\ P_0$.

Based on these plots, the interaction can be roughly divided into three parts which are reported in figure 5 :

- In the initial region of the interaction, hereafter referred to as region A, P^* increases very rapidly from 0 to $0.8P_0$ over a distance of $0.3L$. This increase is produced by the separation shock and is also associated with the large peak of the RMS pressure fluctuations due to the low-frequency shock motions found in the laboratory frame.

- In the region labelled B, downstream of the separation point with $0.2 < X^* < 0.6$, the mean pressure increases slowly, despite no clear plateau, as often reported in largely separated flows[43]. These authors however note that for interaction still resulting in a sizeable separation, the wall pressure distribution displays only an inflection point, as for the present case. Nearly constant RMS pressure fluctuations are also observed in that region.

- Further downstream, in the region C defined by $0.6 < X^* \lesssim 1$, a nearly constant pressure gradient is observed, with an increases of $0.5P_0$ over a distance of L. An overshoot of the RMS pressure fluctuations is also found in this region.

This splitting is confirmed when considering the low-frequency links between the shock displacement and the wall-pressure fluctuations. Large coherence coefficients between the shock displacements estimated at a given altitude and pressure fluctuations in the shock region as well as with downstream regions have been found in figure 4. These results are supplemented by figure 6 where the coherence between the wall-pressure fluctuations and the shock displacements at each altitudes is shown for the frequency such as $S_L = 0.03$. Note that the altitude reported on the y-axis is normalized by the altitude of the crossing point H_I between the incident and separation shocks, as sketched in figure 1(b). The following results can be derived:

- In the region corresponding to the region A defined above, the coherence level is high between the shock displacements and the pressure variations occurring at the separation-shock foot, whatever the shock altitude taken as reference.

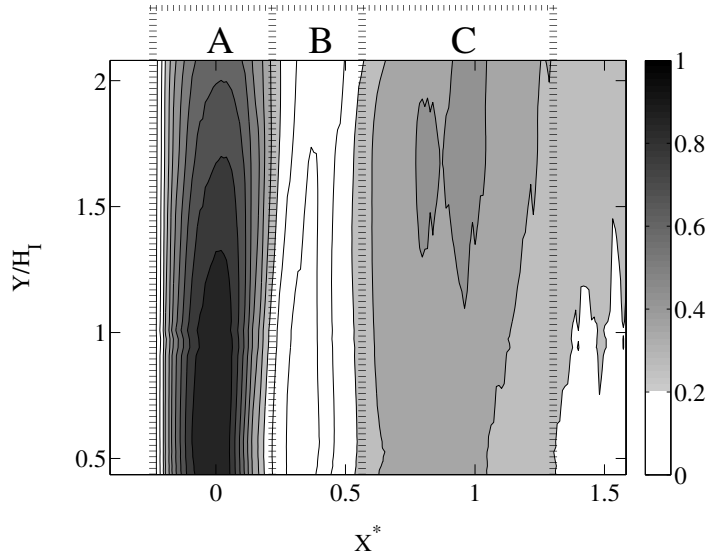

FIG. 6. Coherence for $S_L = 0.03$ between the wall-pressure fluctuations at the normalized streamwise location X^* and the separation-shock displacement at the normalized altitude Y/H_I

.

- High coherence levels are also found between the shock displacements and the pressure fluctuations occurring in the second part of the separated zone that matches region C. Moreover, it is of importance to note that the coherence level increases with the shock altitude.
- The region where the coherence level are the lowest, located between the two previous ones, corresponds to the region B as defined from figure 3.

The accurate matching of regions defined from figures 5 and 6 makes clear that different mechanisms are at play in the interaction and influence the low-frequency unsteadiness of the shock. They seem to be associated with three different regions of the interaction. In order to clarify each mechanism, a conditional analysis of the pressure fields, based on the separation bubble unsteadiness, is presented in the next section.

B. Conditional analysis based on the bubble unsteadiness

The strong differences found for the pressure RMS values and the coherence maps when moving from region A to C suggest that different behaviours are observed in the initial part and in the last part of the interaction. However, as seen in figure 5, the large fluctuations in the initial region of the interaction are induced by the kinematics of the separation shock and are therefore irrelevant when analysing the intrinsic bubble unsteadiness. The separation-shock reference frame is consequently considered throughout this section.

A first attempt to describe the mean and turbulent wall-pressure was developed in Debiève and Dupont[23]. These authors proposed to relate an unsteady pressure gradient downstream the separation shock to the observed phase relationships between pressure fluctuations recorded close to the separation-shock foot and the downstream regions. Unfortunately, this model was derived only from wall-pressure measurements, and could not take into account all the results derived from the present LES data analysis. Therefore, this approach will be revisited by taking into account new possibilities offered by the numerical database regarding the detection of instantaneous location of the separation shock.

In order to understand the links between the unsteady pressure fluctuations, related to the shock displacement, and the pressure fluctuations in the separated zone, the analysis of the pressure fluctuations are conditioned using the low-pass filtered time evolution of the

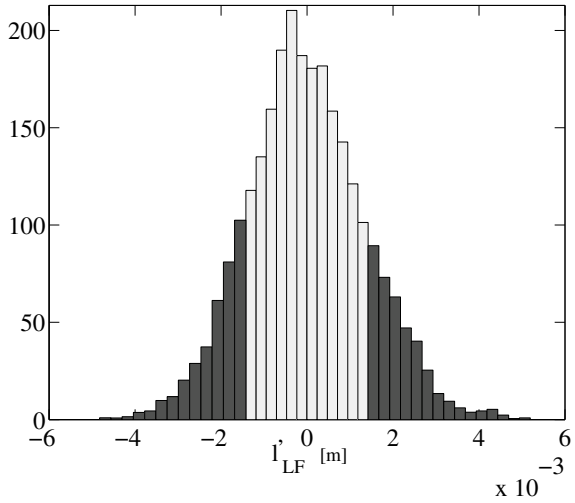

FIG. 7. Probability Density function of the estimated shock location at the altitude denoted by a star in figure 4.

separation-shock location. Note that the separation-shock motion is somehow equivalent to the motion of the separation point s since, for the altitude at which the shock motion is sampled, the shock location is partly driven by Mach waves coming from the vicinity of the separation point, as illustrated by the high level of coherence at low frequency found in vicinity of the separation in figure 4[25]. The shock location is determined at each time step and then low-pass filtered but only 30% of the samples are then considered for the conditional averaging with $2\times15\%$ corresponding to samples where the shock location is the most upstream and the most downstream, respectively. These two classes are highlighted in grey in figure 7 where the probability density function of the low-frequency separation-shock displacements l'_{LF} is plotted.

Piponniau *et al.*[20] have shown that statistically the size of the separated region is directly linked to the location of the separation shock: the bigger the separation bubble is, the more upstream the shock is located. This feature has been also found in the present LES and is consistent with the analyse of Agostini *et al.*[25] demonstrating that, for the altitude at which the shock motion is sampled in the present work (see figure 6), the shock location is set through Mach waves coming from the vicinity of the separation point.

From a practical viewpoint, it is easier to consider the time evolution of the separation-shock location rather than the time evolution of the separation point since the latter one is rather noisy, even if low-pass filtering is considered. This is a consequence of the three-dimensional effects encountered in the vicinity of the separation point, which, though being of lower magnitude than in the reattachment region, result in significant spanwise variations of the separation point. Such three-dimensionality is however smoothed when transmitted up to the separation-shock through Mach waves. Consequently the time variation of the separation-shock location is less subject to these modulations in space and reflects rather accurately the global low-frequency unsteadiness of the bubble. As a consequence, the probability density function shown in figure 7 can be reasonably associated with the low-frequency shock displacement as well as with the low-frequency bubble breathing: negative/positive shock displacements correspond to larger/smaller bubbles, respectively.

In order to evaluate the pressure fluctuations in the separation-shock frame, for each time sample belonging to one of the two aforementioned conditional subsets, the wall pressure is considered at a location translated of the class-averaged shock location associated with the corresponding class and then averaged. The resulting conditional streamwise distribution of wall pressure for small and large bubble are reported in figure 8(a), alongside with the difference between them in figure 8(b). The dimensionless longitudinal coordinate is defined

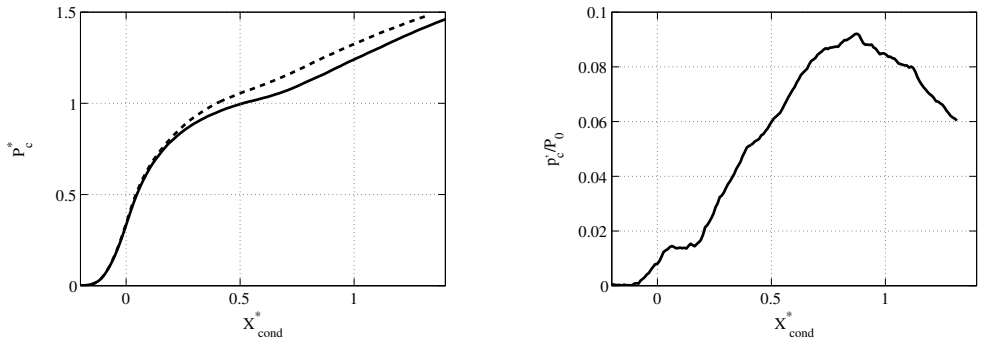

FIG. 8. (a) Conditional pressure distributions for small (dashed line) and large solid line interactions. (b) Difference between the conditional pressures of small and large separation.

by $X^*_{cond} = (x - X_{0,cond}/L)$, where $X_{0,cond}$ is the mean position of the separation-shock foot related to the classes. The main values $P^*_C = (P_C - P_0)/P_0$, where P_C is the average values of the conditional pressures, is denoted on figure 8(a) by the dashed line for the smallest interaction, and full line for the other case. In the frame of the separation shock, the pressure variations $p'_C = \Delta P_C$ is free from the effects of both the translating pressure jump and the incoherent turbulent fluctuations. It is consequently the pressure variation inherent to the dynamics of the bubble, *i.e.* the coherent fluctuations.

- within the upstream part of the bubble ($0 < X^*_{cond} < 0.2$, lying in the region A defined in the wind-tunnel frame of reference), the mean pressure distributions of each case are superimposed. It means that the pressure jump across the separation shock remains nearly constant, being unaffected by the low-frequency breathing of the bubble. This is consistent with previous observations at low frequencies presented in section III and figure 3, where low RMS pressure levels were observed downstream the separation shock closely above the edge of the boundary layer.
- downstream of the separation point ($0.2 < X^*_{cond} < 0.6$, matching the region B in the wind-tunnel frame of reference), the difference between the mean pressure profiles increases continuously, with higher pressure values for the shallow bubble.
- For $0.6 < X^* < 1.2$ (associated with the region C), a maximum of fluctuations is reached ($p'_C/P_0 \simeq 0.09$),
- further downstream, the difference between both classes decreases.

Focusing on the upstream part of the bubble, as the separation-shock intensity remains nearly constant whatever the bubble size, the initial part of the interaction can be approximated as a simple translation of the separation point with a nearly constant flow deviation with the separation shock following this displacement. Note that this proposal differs from the one proposed by Touber and Sandham[17] where the shock motions are directly related to shock angle variations. Beyond that region there is no clear pressure plateau but the streamwise evolution is closer to isobaric for the large bubble, making p'_C increases continuously. Then, in the region $0.6 < X^* < 1.2$, the maximum value of $p'_C/P_0 \approx 0.09$ is reached. This corresponds to $p'_C/P_0 \approx 4 \times p^*_{LF}$, as deduced from the corresponding region in figure 5. Such a value is close to the one obtained by assuming a Gaussian distribution for the low-pass filtered pressure fluctuation that yields typical extremal values of $\pm 3 \times p'_{LF}$. This acceptable concordance demonstrates that the present conditional analysis is consistent. Eventually note that these strong wall pressure fluctuations, transmitted to the supersonic region of the interaction, are able to affect the upper part of the separation shock through the characteristics[30]. This point will be addressed in section V.

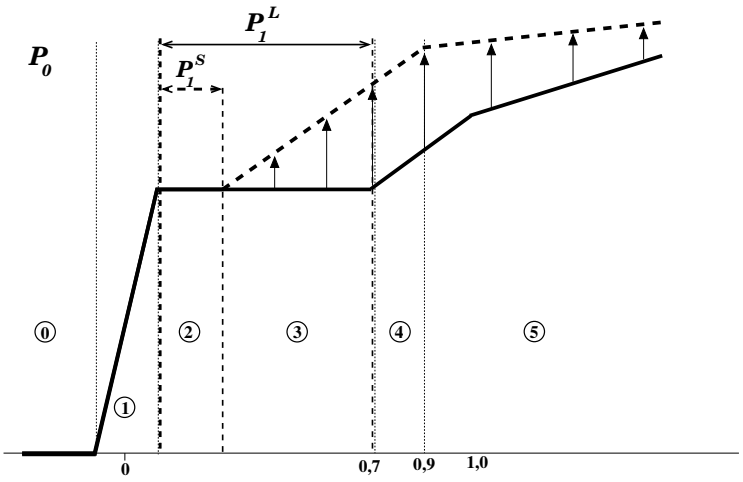

FIG. 9. Scheme of the conditional wall-pressure for shallow (dashed line) and large bubbles (solid line) in the separation-shock frame. The x-axis coordinates are normalized by L.

C. Global scheme for the wall-pressure fluctuations

Taking into account the results described in the previous section, a quasi-static scenario for the evolution of the wall pressure from small to large bubbles is derived from the results detailed in the previous section. It is described in the separation-shock frame in figure 9 with the interaction being split in six regions:

- the upstream region is denoted *0*.
- the pressure jump across the separation shock corresponds to the region *1*.
- the region *2* corresponds to the region where the pressure evolution is isobaric for both small and large bubble. Note that even though no clear isobaric region is found from the present data, it could be observed in cases of more intense separations.
- the region *3* corresponds to the end of the isobaric region for the large bubble and to the beginning of the pressure gradient found in the interaction for the shallow bubble.
- the region *4* corresponds to the region where a nearly constant adverse pressure gradient is found for both small and large bubble.
- finally, region *5* corresponds to the downstream region with vanishing adverse pressure gradients.

The same scheme is sketched in the wind-tunnel frame in figure 10 and the induced phase relationships between the separation-shock location and wall-pressure variations are reported, when defined, in the grey regions. This simple sketch enables to describe the main features of the wall-pressure fluctuations put into light in the previous sections, namely:

- the anti-phase relationship in region A, with large intermittent pressure fluctuations related to the pressure step across the separation shock.
- the in-phase relationship in region C and downstream, as long as the adverse gradient pressure does not vanish, with an overshoot of the coherent pressure fluctuations in region C
- a buffer zone, corresponding to the region B where in-phase, anti-phase or null coherent pressure fluctuations can be obtained. As already mentioned, in our case, the region of isobaric region for shallow bubble is vanishing and the extend of the region

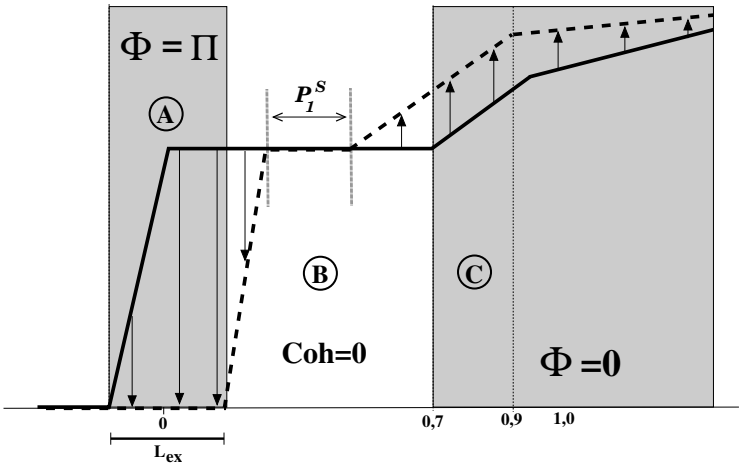

FIG. 10. Scheme of the conditional wall-pressure for shallow (dashed line) and large bubbles (solid line) in the wind-tunnel frame. Grey zones denotes the regions in which a constant phase Φ between the shock location and the pressure can be derived from the scheme. The x-axis coordinates are normalized by L.

bounded by black vertical lines in figure 10 is nearly reduced to a point. Therefore, in region B, we observe mainly equiprobable switches from in-phase to anti-phase, and vice-versa. This is the reason why no correlation between the wall pressure and the shock motions is obtained in this region. Moreover, in the downstream part of this region, coherent pressure fluctuations should increase from nearly null fluctuations to values of the same order than the ones in the region C, as it is observed in figure 8.

The scheme of figure 10 makes it possible to describe the various levels of pressure fluctuations, phase relationships and levels of coherence at the wall along the interaction. These properties have been shown in section III and figures 3 and 4 to be maintained in large regions of the interaction, in particular in the supersonic regions. It will be checked in the next section the ability of this scheme, derived from wall data, to be extended to the supersonic part of the interaction

V. PRESSURE UNSTEADINESS IN THE SUPERSONIC REGION DOWNSTREAM OF THE SEPARATION SHOCK.

The conditional streamwise pressure profiles can be analysed in the supersonic region of the interaction by using the same approach than previously described in section IV B for the wall pressure. The region considered is located above $y = H_I$, *i.e.* over the crossing point of the incident and separation shocks, in order to focus on the outer, supersonic part of the flow. The same two conditioning classes as for the wall pressure are use, corresponding respectively to shallow and large bubbles and the conditionally-averaged pressure at the same dimensionless altitude $Y/H_I = 1.3$ are reported in figure 11. The solid and dashed lines correspond to large and small bubbles, respectively. The origin for the longitudinal coordinate is set to the mean location of the incident shock at the same altitude, denoted X_1.

The pressure immediately downstream the incident shock is nearly constant for both cases, demonstrating that the separation-shock intensity can also be considered as nearly constant in this region. A second pressure bump is found just upstream of the expansion wave, whatever the interaction size, and its intensity increases in the case of little bubbles. The pressure difference upstream of the expansion wave between the shallow and large bubbles is about $6.9 \times 10^{-2}\ P_0$ and it is maintained beyond the expansion fan. Therefore the intensity of the expansion wave can be considered as independent of the state of separation.

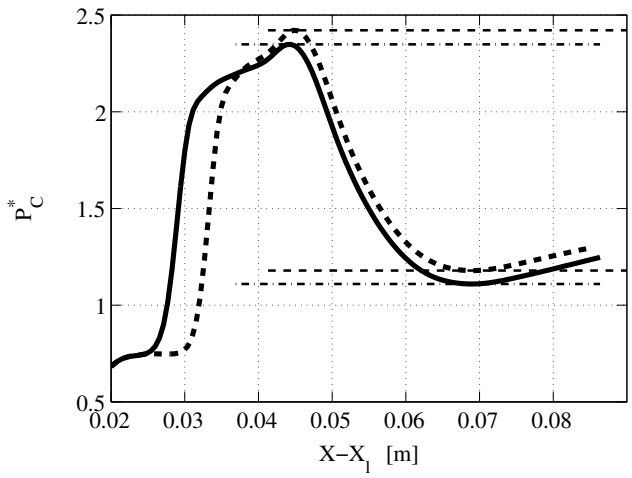

FIG. 11. Conditional mean pressure profiles obtained at $Y/H_I = 1.3$ for shallow (dashed line) and large (solid line) bubbles.

The second pressure bump has to be associated with the crossing of compression waves which are developing between the separation shock and the expansion wave, see figures 1(a) and 3. As previously mentioned, they emanate from the reflection of the incident shock on the sonic line[37], denoted by the dashed line in figure 3.

At this point of the analysis, it seems that the pressure fluctuations in the external flow follow the dynamics of the separated region. As the external flow is supersonic relative to the separated region, pressure perturbations will spread out along the directions defined by the characteristics[30]. This implies that low-frequency pressure fluctuations emanating from the region B can influence the separation-shock region up to its intersection with the compression waves, denoted H_w in figure 1(b), while the one emanating from region C will influence the shock above H_w.

It has been found in previous sections that significant coherent pressure fluctuations are encountered in the separated region only downstream of the beginning of region C. Consequently the shock system remains nearly constant below H_I. On the opposite, coherent pressure fluctuations developing in the downstream part of the region B and in region C lead to an increase of the pressure for shallow bubbles. The beginning of region C corresponds to the reflection of the incident shock on the shear layer. As this one experiments low-frequency fluctuations of its upstream condition, the intensity of the reflected compression waves, created just upstream of the expansion wave, is also modulated at low-frequency. Since it is seen in figure 11 that the pressure difference between the two conditional means remains constant throughout the expansion fan, it implies that the low-frequency pressure fluctuation in the supersonic region are in phase with their subsonic counterparts in region C. Eventually, the compression waves merge with the separation shock for $Y > H_w$. It suggests that in that region the shock system has a variable intensity related to the size of the interaction: the separation-shock intensity remains nearly constant, but it is strengthened by the compression waves. As the compression-wave magnitude depends on the bubble-size state, the pressure both increases across the equivalent shock and is regulated by the bubble breathing.

In the next section, a conceptual, inviscid, view of the low-frequency unsteadiness developing the interaction is proposed. It is built in order to take into account all of the features described thus far.

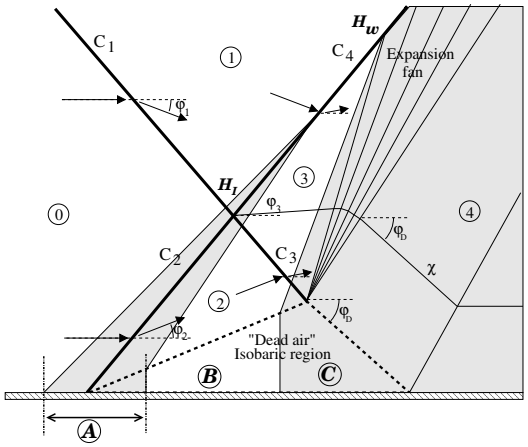

FIG. 12. Inviscid equivalent scenario for shock-wave boundary layer interaction with separation[43].

VI. CONCEPTUAL MODEL OF EQUIVALENT INVISCID INTERACTION

A. Reminder: free interaction theory

An inviscid equivalent scheme of the shock-wave/boundary-layer interaction has already been proposed by Delery[43] and is sketched in figure 12. The separation region is assimilated with an isobaric region divided in two parts:

- the upstream one extends from the separation point to the reflection of the incident shock on the separated region. This region corresponds to a constant positive deviation angle.
- The downstream region is associated with a constant negative angle so as to insure the flow reattachment, resulting in the creation of the expansion wave. Pressure equilibrium between the isobaric separation and the supersonic regions is obtained by ensuring that the pressure decreases across the expansion wave is equal to its increase across the incident shock. Thus, the expansion deviates the flow down to the wall of an angle approximatively equal to the incident shock and $P_2 \simeq P_4$.

Downstream of the reattachment, an equivalent reattachment shock is required to model the flow deviation required to achieve wall-parallel streamline. It results in the pressure increase found downstream of the interaction. When the interaction is fully separated, the deflection angle imposed by the first ramp becomes independent of the incident-shock intensity and consequently the pressure ratio at the separation point as well. Close features were also found for compression ramps[44], in agreement with the so-called *free interaction theory*[45].

It was shown in section IV that the whole separated region can not be associated with an isobaric region since the initial region only exhibits a pressure gradient close to zero. In the second part of the separated region, a significant adverse pressure gradient is developing and is associated with large unsteady pressures. Moreover, it has been shown in section V that the shock system equilibrates the pressure between the subsonic and supersonic regions by means of reflected compression waves produced by the reflection of the incident shock through the boundary layer[37]. Such compression waves, seen in figure 1(a) as dark lines located upstream of the expansion fan, are inconsistent with a single ramp scenario as described in figure 12.

A new conceptual model, sketched in figure 13(a) is introduced to alleviate these shortcomings. A new second ramp is added just upstream of the impingement point of the incident-shock. It splits the equivalent subsonic region into two parts which can respectively be associated with regions B and C of the scheme introduced in figure 10. The first

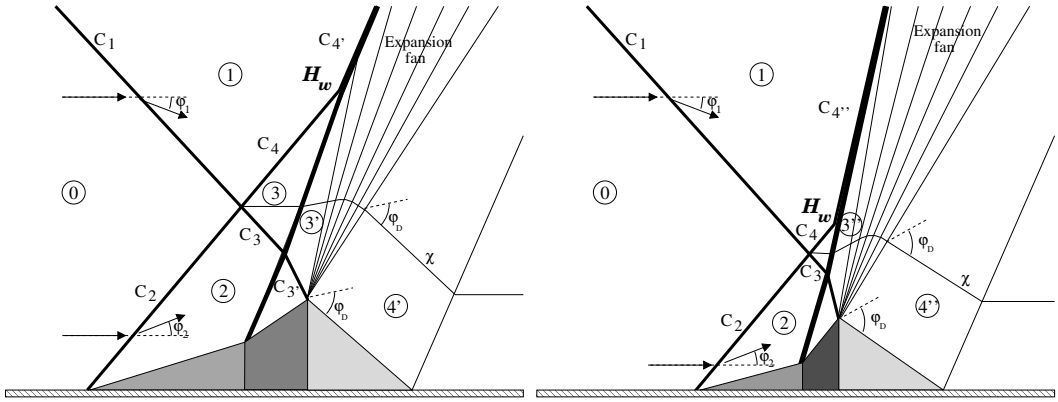

(a)Large separated region (b)Small separated region

FIG. 13. Possible inviscid equivalent scenario of the shock wave boundary layer interaction depending on the interaction length.

ramp results in a flow deflection compatible with the *free interaction* theory, *i.e.* independent of the size of the separation. The flow then undergoes a second deviation due to the second ramp which imposes a pressure increase. In the inviscid supersonic region, this leads to the creation of the shock C_3' which intersects the separation shock C_4 near H_w, thus strengthening the separation shock up to the value C_4'. In the next section, this conceptual model is extended to include the different states of the subsonic separated bubble.

B. Description of the quasi-static scenario

Results described in section V bring out that the intensity of the equivalent shock C_3' depends on the bubble size: its intensity, or equivalently the flow deviation of the second ramp in the model, decreases when the bubble is expanding and vice versa. The figure 13(a), being from now on associated with large bubbles, is consequently complemented by figure 13(b), which corresponds to small bubbles. Considering a growing bubble, the dynamics of the interaction can be modelled in the following quasi-static way:

- the separation point is translated in the upstream direction, with a constant flow-deviation angle and a translation velocity negligible with respects to the upstream velocity.
- as the deviation angle does not change and as the translation velocity is low, the separation-shock intensity remains constant. The shock is therefore simply translated in order to follow the motion of the separation point.
- Within the second part of the bubble, the pressure gradient weakens, as seen in figure 8(b).
- As the pressure decreases, the compression-wave arising from the refraction of the incident shock through the mixing layer weakens.
- As the expansion wave does not change, the pressure behind the shock system is also reduced.
- The reattachment shock finally ensures that the flow turns parallel to the wall and then equilibrates the downstream pressure

The inverse procedure is developing when the bubble is contracting.

Such a scenario extends to the supersonic regions the scheme built from the wall pressure in figure 10. It also describes the unsteadiness features of the interaction and explains how

the shock system depends on the separated zone. It is also consistent with the coherence map of figure 4: large coherence is observed between the low-frequency shock displacements (or bubble breathing) and the expansion, compression waves, as well as the downstream supersonic regions. On the opposite, in the intermediate region, upstream of the compression waves, no correlation, and limited pressure fluctuations is observed.

The low-frequency unsteadiness of the first ramp can be associated with the bubble breathing, which is associated with the extent of the region B having a small or null pressure gradient (isobaric region in cases of large separated bubbles). This is the origin of the longitudinal displacements of the separation shock, and could be explained by imbalanced mass flux across the initial part of the mixing layer[20]. On the other side, the second ramp unsteadiness involves a specific region of the interaction, typically $0.6 < X^* < 0.8$, see figure 8. This one corresponds to the region C, where large pressure gradients are observed, downstream of the nearly isobaric region, as in subsonic separated cases. This pressure gradient ensures the connection with the downstream pressure of the separated region and generates weak pressure fluctuations at low frequency, as proposed by the schemes in figure 13.

VII. DISCUSSION

This conceptual model enables to describe the streamwise evolution of the pressure as a function of the interaction length but it is restricted to low-passed-filtered data. However several authors have pointed the importance of the convective structures produced by the shear layer induced by the decelerated region in the mechanism which generates the low-frequency unsteadiness, for incompressible flows[46–48] as well as for compressible ones[49]. As a consequence, the compatibility of the model with the medium-frequency unsteadiness (Strouhal number ranging from 0.5 to 1.0) will be considered in this section. It will be checked if this model introduced previously for describing the different pressure variation features in incompressible flow can be extended to compressible flow.

A. Attempt to establish similarity between incompressible and compressible separation bubbles

Several experiments as well as numerical simulations have shown that large structures are developing in the shear layer downstream the separation shock. The spatial development of these structures has been compared with incompressible separated flows and large similarities were highlighted[5], with two distinct frequency ranges in the upstream part of the separated region (the region B introduced in this paper) and the downstream part (region C). This second region was associated with the development of large structures being shed downstream, as in subsonic cases. A typical Strouhal number $S_L \simeq 0.5$ was associated with the frequencies of the shedding, typically one order of magnitude higher than the low frequencies of the shock motions ($S_L \simeq 0.03$). Evidences of low-frequency variations of the typical velocity profiles and wall shear stress related to some large coherent scales were also found in the case of a Mach 2.9 compression corner with separation[16]. Piponniau *et al.*[20], developed a model which links the mass entrainment associated with the development of these structures to the low-frequency breathing of the separated region, an idea already suggested in several subsonic works[50–52]. This model is suited for incompressible as well as compressible separated flows despite it underlines the large effects of compressibility on the low-frequency unsteadiness. These various results suggest that large similarities are observed between incompressible and compressible separated flows. In the present work, the pressure-field analysis makes it possible to put an additional sight on these similarities.

Lee and Sung[53] have compiled several results obtained for separated subsonic flows obtained for backward step flows. The corresponding streamwise RMS and mean pressure distributions are reported in figure 14. The pressure fluctuations have been normalized by the upstream dynamic pressure q_0. In order to compare with the present results, figure 14 is zoomed and centred on the separated region displayed in figure 8 and corresponding to

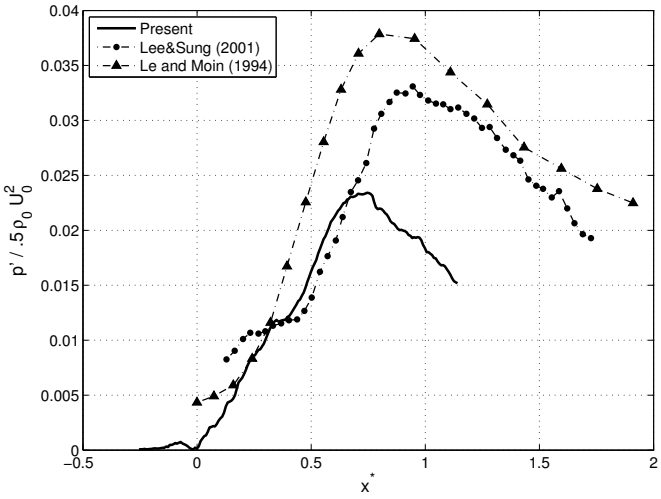

FIG. 14. Streamwise evolution of the RMS pressure in separated flows. Solid line: present work; dashed-dotted lines: subsonic backward facing steps from experiments[53] (•) and DNS[54] (▲).

regions B and C. The coherent pressure fluctuations are normalized with the dynamic pressure obtained downstream of the incident shock C_1. The dimensionless longitudinal coordinate X_{sep} is defined by $(x - X_0)/L_{sep}$, where L_{sep} is the length of separation and X_0 the separation point, associated with the mean position of the separation shock in the compressible case.

The different subsonic cases reported in figure 14 correspond to various backward facing steps. Two important points can be emphasized. First, the subsonic measurements are given in the wind-tunnel frame. Nevertheless, in cases of backward facing steps, the separation point is fixed at the corner of the step. Therefore, the conditional analysis developed in the previous section, which tries to remove the influence of the moving the separation point associated with the separation-shock displacements, make it possible to compare the present compressible conditional analysis with an incompressible compilation[53]. The second point to note is that only the coherent part of the pressure fluctuations has been evaluated, while subsonic results correspond to broadband measurements: therefore, the level of fluctuations cannot be directly compared on an absolute basis.

Nevertheless, it is clear that large similarities can be observed between compressible and incompressible cases. In both cases, the separated region is split in two parts, as suggested by the scheme in figure 9:

- the upstream part with limited pressure gradient, associated with the inflection point in the pressure distribution, as well as weak pressure fluctuations (in region B),
- the downstream part, characterized by a stronger adverse pressure gradient related to strong pressure fluctuations (in region C).

The matching between the scheme of figure 9 and subsonic experiments[53] is even better than for the present compressible SWBLI since nearly constant RMS values are encountered downstream of the separation point. This is probably due to the fact that this separated flow exhibit clear *plateau* pressure in the region B while the SWBLI under consideration is not sufficiently separated to develop such a well defined *plateau* region, see discussion in section IV B.

Reasonably, region C seems to be related to the development of large coherent scales, shed downstream of the interaction, and associated with the large turbulent pressure fluctuations occurring in that region. It can therefore be reasonably assumed that the dynamics of the large coherent scales along the shear layer is associated with the coherent pressure

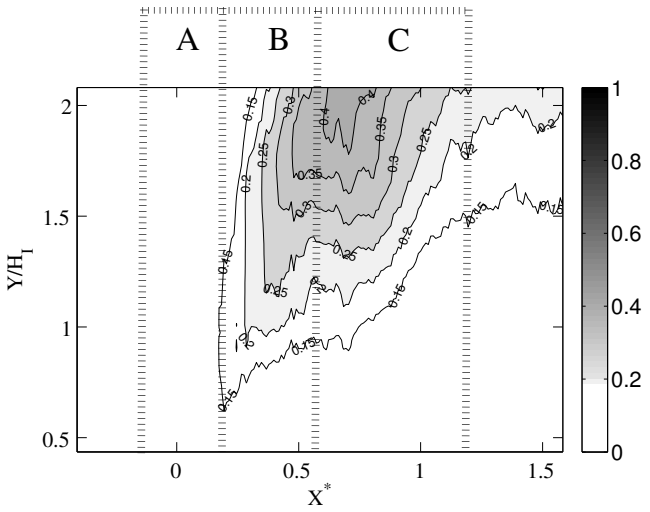

FIG. 15. Coherence for $S_L = 0.5$ between the wall-pressure fluctuations at the normalized streamwise location X^* and the separation-shock displacement at the normalized altitude Y/H_I.

fields shown in figure 14. Consequently a reasoning analogous to the ones related to the low-frequency bubble breathing could describe the influence of the pressure fluctuations associated with the coherent scales ($S_L \simeq 0.5$) on the shock displacement at medium frequencies. This point is addressed in the following section.

B. Generalisation of the inviscid model to medium frequencies

Previous works[30,55], bring out that within the shear layer, organized convective structures are produced and are associated with Strouhal number ranging from 0.5 to 1.0. These structures convect with a supersonic velocity relative to the supersonic side of the interaction and the pressure disturbances generated by the convective structures as well as the propagation paths have been clearly defined. These results are summarized in figure 15 by the map of the coherence at $S_L = 0.5$ between the longitudinal shock motion at given altitudes and the wall pressure at given streamwise locations. It sheds light on the links between the separation-shock displacement and the medium-frequency pressure fluctuations induced by the convective structures, in a similar way as figure 6 did for the link between the shock motion and the low-frequency unsteadiness.

- In the first part of the interaction, the structures produced by the shear layer are convected, and the pressure disturbances affect the separation-shock dynamics. Throughout their displacements in the region $X^* < 0.5$, the pressure fluctuations produced by the convective structures propagate along Mach waves and influence the region below the crossing point between the separation shock and the expansion waves. It is consistent with the fact that the coherence coefficient increases with the altitude in the region B, as seen in figure 15.

- In region C, the wall-pressure variations and the separation-shock dynamics have the strongest coherent-coefficient level at high altitude. It has to be noted that any modulation of the upstream conditions of the lower part of the incident shock will affect its reflection in compression waves so as to balance the pressure fields imposed by the subsonic region[30,37]. Consequently the large coherent scales developing in region B and then crossing the adverse pressure gradient found from the beginning of region C are modulating the separation-shock intensity through the compression

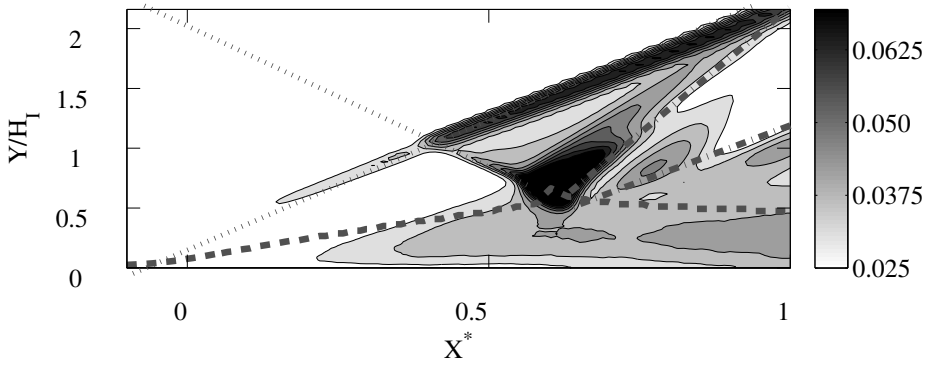

FIG. 16. RMS range-filtered pressure fluctuations corresponding to medium frequency with Strouhal numbers ranging from 0.3 and 0.8. The Mach line is denoted by a dashed line. The dotted line corresponds to the incident and separation shocks and the dashed-dotted lines mark the boundaries of the expansion fan.

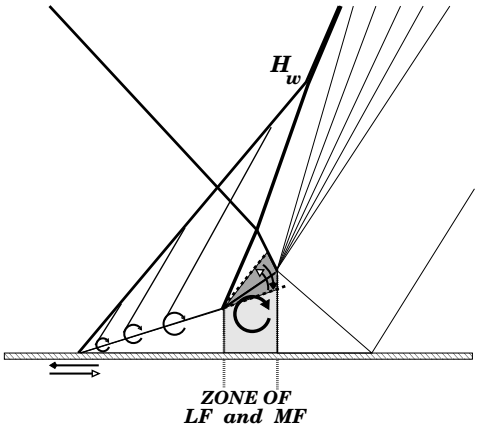

FIG. 17. Conceptual inviscid model of sources for the low and medium frequency unsteadiness in the interaction

waves propagating just upstream of the expansion fan. It results in the aforementioned high level of coherence seen in figure 15.

The influence of the medium-frequency coherent structures on the reflection of the incident shock can be verified by looking at figure 16 where RMS pressure values for the medium-frequency range $0.3 < S_L < 0.8$ are reported. Average values induced by the convection of the coherent structures along the mixing layer are found in region B while the foot of the incident shock/reflected compression waves experiences much higher values. Large values are also recovered along the path of the compression waves up to the location H_w at which they intercept the separation shock.

Based on these findings, the inviscid equivalent model sketched in figure 13 can be extended to the medium-frequency unsteadiness by linking the medium-frequency unsteadiness to the second ramp in order to include the pressure variations due to the interaction of the convective structures with the adverse pressure gradient of region C.

It may be noted that it has been found[5] that the characteristic frequencies associated with the Kelvin-Helmholtz-like structures developing downstream of the separation point experience an abrupt decrease when they approach of region C: the associated Strouhal number was found to decrease from values about 1 in the region B to a constant value of 0.5 in the region C, whatever the flow deviation. Similar results were also found for a

transonic compression-corner flow[2] as well as for subsonic separated flows[48]. This feature was explained by the occurrence of some structure amalgamation phenomena in the mixing layer near the region C, leading to larger eddies shed into the downstream flow. The flow deviations and higher pressure fluctuations induced by this non-linear process would consequently be related to the mechanism leading to the maxima of pressure fluctuations at medium frequency in this vicinity as seen in figure 16. The fact that such unsteadiness seem also to occur in low-Mach number separated flows is another illustration of the similarities between incompressible and compressible separated flows highlighted in section VII A.

The newly-defined model encompassing both the low- and medium-frequency phenomena is illustrated in figure 17. The first ramp (region B) follows the low-frequency unsteadiness of the separation point (region A), and convective structures are developing in this region, influencing the separation shock through the Mach lines[30]. When these structures enters the vicinity of the second ramp (region C), their dynamics changes abruptly. These variations could be linked to the pressure gradient induced by the second ramp, and the intensity of the second ramp could be affected in return by the new convective-structure dynamics. Therefore, the second ramp, associated with the region C in the scheme 17, oscillates with two characteristic frequencies:

- a low one, with $S_L \simeq 0.03$, associated with the bubble breathing,
- a medium one, with $S_L \simeq 0.5$, associated with the convective structures and the rapid decrease of their time scale in this region.

The resulting unsteady pressure field at low and medium frequency compares well with the LES data taking into account the fact that the outer flow unsteadiness derive from the unsteadiness in the subsonic region through the characteristic theory[30]. In particular, the phase relationships, the coherence maps and the evolution of the pressure standard deviation are qualitatively reproduced.

It may be stressed that the present scheme does not explain the origin of the low-frequency unsteadiness. This one could be induced by the medium frequency unsteadiness, as suggested by several authors both for subsonic[48,51,56] and supersonic[16,20] flows. However no direct link between the low-frequency unsteadiness of the interaction and the convective structures of the mixing layer at medium frequencies have been so far established for the present flow. Nonetheless, whatever the precise mechanism that may relate the two frequency ranges, the proposed simple inviscid scheme will describe accurately the whole field of unsteady pressure within the interaction and downstream of it.

VIII. CONCLUSION

Large Eddy Simulations of a Mach 2.3 shock reflection on a turbulent boundary layer have been achieved for flow deviations leading to separated interactions. Long time computations allowed to describe more than 150 cycles of the low-frequency unsteadiness of the interaction, characterized by a Strouhal number roughly equal 0.03. The numerical results have been shown to describe accurately the low- and medium-frequency unsteadiness of the flow when compared with experimental data obtained in the same aerodynamic conditions.

Frequency and conditional analyses of the pressure fields have given a global overview of the space-time organisation of the flow. Based on these data, an equivalent inviscid scheme is introduced and is summarized by figure 17. It allows the reproduction of the essential properties of the pressure variations within the interaction and downstream.

This conceptual model mimics the origins of the shock-system unsteadiness at low frequencies ($S_L = 0.03$) as well as medium frequencies ($S_L = 0.5$). The displacement of the upstream part of the separated region is described as a simple corner translation, hence the separation shock induced by this flow deviation moves with a closely constant intensity. The second part of the separated zone is the source of pressure fluctuations which influence the supersonic region of the interaction. This second part is described as a second unsteady flow deviation depending on the bubble size, although the physical nature of mechanism inducing these fluctuations remains an open question. This scheme is nonetheless able to

give a justification for the different regions identified from the RMS pressure fields and coherence function with the shock motions.

Moreover, it is shown that the separation-shock experiments only a translation motions with negligible variation of its intensity. Nevertheless, in the region located above the intersection with the incident shock, the separation-shock intensity is strengthened by the merging of unsteady pressure waves which are emitted from the shedding region at low and medium frequencies. It generates unsteady pressure fluctuations downstream of the expansion wave that are in phase with the displacement of the separation shock.

The proposed scenario puts into light the possible interaction between the bubble breathing at low frequency and the convective structures associated with the medium frequencies. Such an interaction should arise in the second part of the interaction, in the region of the reattachment point, as sketched in the inviscid model by a ramp imposing a flow deviation at low frequency as well as at medium frequency. It is of importance to specify that the effects induced by the flow deviation in the inviscid model could be generated by other, viscous, mechanisms in a real flow. Such mechanism could include a modulation at low frequency of the dynamics of convective structures or a non-linear coupling between the long-term variation of the pressure gradient associate to the second ramp with the short-term variation of convective structure. It seems therefore that a detailed, statistical, space-time description of these convective structures could be a key point for understanding the low-frequency unsteadiness in separated flows. This remark holds for incompressible as well as compressible flows since it appears from the present work that the shock-system unsteadiness is merely a passive "slave" of the dynamics developed in the separated region.

IX. ACKNOWLEDGEMENTS

This work was partly supported by the Agence National de la Recherche (ANR) through the DECOMOS project from the program Blanc. It was granted access to the high-performance computing resources of Institut du Développement et des Ressources en Informatique Scientifique (IDRIS) under allocations 2009-021877 and 2010-021877 made by Grand Equipement National de Calcul Intensif (GENCI).

[1]M. E. Erengil and D. S. Dolling, AIAA Journal **29**, 728 (1991).
[2]F. O. Thomas, C. M. Putman, and H. C. Chu, Experiments in Fluids **18**, 69 (1994).
[3]D. S. Dolling, AIAA Journal **39**, 1517 (2001).
[4]S. J. Beresh, N. T. Clemens, and D. S.Dolling, AIAA Journal **40**, 2412 (2002).
[5]P. Dupont, C. Haddad, and J. F. Debiève, Journal of Fluid Mechanics **559**, 255 (2006).
[6]B. Ganapathisubramani, N. T. Clemens, and D. S. Dolling, in *45th AIAA Aerospace Sciences Meeting and Exhibit, Reno, Nevada* (2007).
[7]M. Wu and M. P. Martin, Journal of Fluid Mechanics **594**, 71 (2008).
[8]E. Touber and N. D. Sandham, Theoretical and Computational Fluid Dynamics **23**, 79 (2009).
[9]B. Morgan, K. Duraisamy, N. Nguyen, S. Kawai, and S. K. Lele, Journal of Fluid Mechanics **729**, 213 (2013).
[10]R. A. Humble, G. E. Elsinga, F. Scarano, and B. W. Van Oudheusden, Journal of Fluid Mechanics **622**, 33 (2009).
[11]R. A. Humble, F. Scarano, and B. W. Van Oudheusden, Journal of Fluid Mechanics **635**, 47 (2009).
[12]L. J. Souverein, B. W. Van Oudheusden, F. Scarano, and P. Dupont, Measurement Science and Technology **20**, 074003 (16pp) (2009).
[13]L. J. Souverein, P. Dupont, J. F. Debiève, J. P. Dussauge, B. W. Van Oudheusden, and F. Scarano, AIAA Journal **48**, 1480 (2010).
[14]P. Dupont, S. Piponniau, A. Sidorenko, and J. F. Debiève, AIAA Journal **46**, 1365 (2008).
[15]E. Touber and N. D. Sandham, Shock Waves **19**, 469 (2009).
[16]S. Priebe and M. P. Martin, Journal of Fluid Mechanics **699**, 1 (2012).
[17]E. Touber and N. Sandham, Journal of Fluid Mechanics **671**, 417 (2011).
[18]K. Plotkin, AIAA Journal **13**, 1036 (1975).
[19]J. Poggie and A. Smits, Physics of Fluids **17**, 018107.1 (2005).
[20]S. Piponniau, J. P. Dussauge, J. F. Debiève, and P. Dupont, Journal of Fluid Mechanics **629**, 87 (2009).
[21]P. Dupont, C. Haddad, J. P. Ardissone, and J. F. Debiève, Aerospace Science and Technology **9**, 561 (2005).
[22]J. P. Dussauge, P. Dupont, and J. F. Debiève, Aerospace Science and Technology **10**, 85 (2006).
[23]J. F. Debiève and P. Dupont, Shock Waves **19**, 499 (2009).
[24]E. Garnier, Shock Waves **19**, 479 (2009).

[25]L. Agostini, L. Larchevêque, E. Garnier, and E. De Martel, in *3rd EUCASS conference, Versailles, France, EUCASS2009-395* (2009).
[26]E. Garnier, P. Sagaut, and M. Deville, AIAA journal **40**, 1935 (2002).
[27]E. Lenormand, P. Sagaut, P. TA, *et al.*, AIAA journal **38**, 1340 (2000).
[28]F. Ducros, V. Ferrand, F. Nicoud, C. Weber, D. Darracq, C. Gacherieu, and T. Poinsot, Journal of Computational Physics **152**, 517 (1999).
[29]M. Pamiès, P. É. Weiss, E. Garnier, S. Deck, and P. Sagaut, Physics of Fluids **21**, 045103 (2009).
[30]L. Agostini, L. Larchevêque, P. Dupont, J. F. Debiève, and J. P. Dussauge, AIAA Journal **50**, 1377 (2012).
[31]L. J. Souverein, B. W. Van Oudheusden, and F. Scarano, in *7th International Symposium on Particle Image Velocimetry, 11–14 September 2007, Rome, Italy* (2007).
[32]L. J. Souverein, B. W. Van Oudheusden, F. Scarano, and P. Dupont, in *38th Fluid Dynamics Conference and Exhibit, Seattle, Washington, USA, AIAA-2008-4169* (2008).
[33]S. Piponniau, E. Collin, P. Dupont, and J. Debiève, International Journal of Heat and Fluid Flow **35**, 176 (2012).
[34]J. F. Debiève and J. P. Lacharme, in *IUTAM Symposium on Turbulent Shear-Layer/Shock-Wave Interaction, Palaiseau, France* (1985).
[35]B. Ganapathisubramani, N. T. Clemens, and D. S. Dolling, Journal of Fluid Mechanics **585**, 369 (2007).
[36]B. Ganapathisubramani, N. T. Clemens, and D. S. Dolling, Journal of Fluid Mechanics **556**, 271 (2006).
[37]L. F. Henderson, Journal of Fluid Mechanics **30**, 699 (1967).
[38]D. S. Dolling and C. T. Or, Experiments in Fluids **3**, 24 (1985).
[39]J. F. Debiève and P. Dupont, in *IUTAM Symposium on Unsteady Separated flows and their Control, Corfu, Greece* (2007).
[40]S. Pirozzoli and F. Grasso, Physics of Fluid **18** (2006).
[41]M. Wu and M. P. Martin, AIAA Journal **45**, 879 (2007).
[42]E. Touber and N. D. Sandham, in *38th AIAA Fluid Dynamics Conference, Seattle, Washington, USA* (2008).
[43]J. Délery, "Shock-wave boundary layer interactions," Tech. Rep. (DTIC Document, 1986).
[44]F. W. Spaid and J. C. Frishett, AIAA Journal **10**, 915 (1972).
[45]D. R. Chapman, D. M. Kuehn, and H. K. Larson, "Investigation of separated flow in supersonic and subsonic streams with emphasis of the effect of transition," Tech. Rep. (1957).
[46]J. K. Eaton and J. P. Johnston, in *Turbulent Shear Flows 3*, Vol. 1 (1982) pp. 162–170.
[47]M. Kiya and K. Sasaki, Journal of Fluid Mechanics **137**, 83 (1983).
[48]N. J. Cherry, R. Hillier, and M. E. M. P. Latour, Journal of Fluid Mechanics **144**, 13 (1984).
[49]S. Piponniau, J. P. Dussauge, J. F. Debiève, and P. Dupont, in *Ictam 2008* (2008).
[50]J. K. Eaton and J. P. Johnston, AIAA Journal **19**, 1093 (1981).
[51]M. Kiya and K. Sasaki, Journal of Fluid Mechanics **154**, 463 (1985).
[52]D. M. Driver, H. L. Seegmiller, and J. Marvin, AIAA Journal **25**, 914 (1987).
[53]I. Lee and H. J. Sung, Experiments in fluid **30**, 262 (2001).
[54]H. Le and P. Moin, "Direct numerical simulation of turbulent flow over a backward facing step. Report no. TF-58," (1994).
[55]L. Agostini, P. Dupont, L. Larchevêque, and J. Dussauge, International Journal of Engineering Systems Modelling and Simulation **3**, 46 (2011).
[56]U. Ehrenstein and F. Gallaire, Journal of Fluid Mechanics **614**, 315 (2008).